Nanoscale

PAPER

View Article Online
View Journal | View Issue

Cite this: *Nanoscale*, 2016, **8**, 14237

A highly sensitive, highly transparent, gel-gated MoS_2 phototransistor on biodegradable nanopaper†

Qing Zhang,[a,b] Wenzhong Bao,[b,c] Amy Gong,[b] Tao Gong,[d] Dakang Ma,[d] Jiayu Wan,[b] Jiaqi Dai,[b] Jeremy N. Munday,[d] Jr-Hau He,*[c] Liangbing Hu*[b] and Daihua Zhang*[a]

Received 24th February 2016,
Accepted 17th June 2016

DOI: 10.1039/c6nr01534d

www.rsc.org/nanoscale

Transition metal dichalcogenides hold great promise for a variety of novel electrical, optical and mechanical devices and applications. Among them, molybdenum disulphide (MoS_2) is gaining increasing attention as gate dielectrics and semiconductive channels for high-performance field effect transistors. Here we report on the first MoS_2 phototransistor built on a flexible, transparent and biodegradable substrate with an electrolyte gate dielectric. We have carried out systematic studies on its electrical and optoelectronic properties. The MoS_2 phototransistor exhibited an excellent photoresponsivity of ~1.5 kA W^{-1}, about two times higher compared to typical back-gated devices reported in previous studies. The device is highly transparent at the same time with an average optical transmittance of 82%. Successful fabrication of phototransistors on flexible cellulose nanopaper with excellent performance and transparency suggests that it is feasible to achieve an ecofriendly and biodegradable phototransistor with great photoresponsivity, broad spectral range and durable flexibility.

Printed electronics with flexibility has attracted tremendous interest in recent years.[1–4] Conventional electronics are made with a glass or plastic substrate. Glass substrates can endure very high handling temperatures[2] but provide poor flexibility. Plastic substrates are transparent and flexible,[5] but they are not environmentally friendly and may take hundreds of years to decompose. Recently, ultra-smooth transparent nanopaper with an optical transmittance over 90% has been developed for flexible electronics.[6–9] Nanopaper is made from the same natural wood pulp material as in paper, while consisting of much thinner nanofibrillated cellulose (NFC) fibers of 5 to 10 nm in diameter.[10–12] The wood fibers are treated with (2,2,6,6-tetramethylpiperidin-1-yl)oxyl (TEMPO)[13,14] to convert the hydroxyl groups to sodium carboxylate groups for improved packing density.[15–18] The fibers are then disintegrated by using a high pressure mechanical homogenizer.[9] The densely packed nanofibers leave a minimal amount of air trapped in the paper and give rise to very high transparency. Their ultra-small diameter also makes the paper surface sufficiently smooth to be used as the supporting substrate for a variety of functional nano-devices. Furthermore, the use of biodegradable natural wood pulp ensures that the device is environmentally friendly at the same time.[1] In a typical CMOS chip, the functional section is formed by only a small portion of the chip, whereas the supporting substrate comprises more than 99% of the semiconductor materials.[19] These ecofriendly transistors can help conserve non-renewable natural resources by replacing toxic semiconductor materials with biodegradable nanopapers.[2]

A phototransistor is essentially a light-sensitive field effect transistor (FET) that transduces the incoming photoenergy to electrical current. Phototransistors based on two dimensional (2D) materials have become increasingly popular in recent years.[20–22] Among them, MoS_2 has received particular interest due to its unique electrical and optical properties.[23–26] In fact, devices made of bulk MoS_2 emerged decades ago.[27–29] Its special band structure, mechanical flexibility and ease of processing make MoS_2 an ideal candidate material for optoelectronics applications.[30] Many groups have reported on MoS_2-based phototransistors fabricated on Si/SiO_2 substrates, which were neither flexible nor environmentally friendly.[31,32] In this work, we demonstrate a flexible, transparent and bio-

[a]*State Key Laboratory of Precision Measuring Technology & Instruments, College of Precision Instrument and Opto-electronics Engineering, Tianjin University, Tianjin 300072, China. E-mail: dhzhang@tju.edu.cn*
[b]*Department of Materials Science and Engineering, University of Maryland, College Park, Maryland 20742-4111, USA. E-mail: binghu@umd.edu*
[c]*Computer, Electrical and Mathematical Sciences and Engineering (CEMSE) Division, King Abdullah University of Science and Technology (KAUST), Thuwal 23955-6900, Kingdom of Saudi Arabia. E-mail: rhau.he@kaust.edu.sa*
[d]*Department of Electrical and Computer Engineering, University of Maryland, College Park, Maryland 20742-4111, USA*
†Electronic supplementary information (ESI) available. See DOI: 10.1039/c6nr01534d

degradable phototransistor gated through a gel-electrolyte. Two sheets of nanopaper are used as the supporting substrate and the top passivation layer to sandwich the MoS_2 channel and the gel-electrolyte in between. We used multilayered MoS_2 as it possesses higher density of states in the conduction band and yields higher photocurrent compared to single layered crystals according to theoretical predictions.[34] We have systematically characterized the electrical and optoelectronic properties as well as the optical transmittance of the phototransistor. The device exhibits exceptionally high photoresponsivity (~1.5 kA W^{-1}) and excellent optical transmittance (~82%).

Fig. 1 illustrates the device structure prior to passivation. 50 nm thick gold electrodes were deposited on the top of a mechanically exfoliated MoS_2 flake through a shadow mask. We chose a shadow mask over standard photolithography to avoid dissolving of the nanopaper with wet processes. The shadow mask also minimizes process-induced contamination and ensures good contact quality between the MoS_2 and metal electrodes. We then coated a thin layer of gel-electrolyte (1 M $LiClO_4$ in w/w = 1 : 10 (ref. 33) polyethylene oxide, see the ESI†) on the top of the MoS_2 flake as the gate dielectric.[34–36] To immobilize the gel-electrolyte and protect the active area, we covered the surface with a separate sheet of nanopaper to form a conformal seal. The entire process flow of the sandwich structure is summarized in Fig. 2A and in the ESI.†

The photograph in Fig. 2B shows a sealed device. The blue dashed line identifies the edge of the top sealing nanopaper. The size is large enough to cover the entire MoS_2 flake and the electrodes, while small enough to expose the metal pads for probing or wire bonding. The microscopy image of Fig. 2C zooms into the active area of the device. The MoS_2 flake at the center serves as the photo-sensitive channel. An atomic force microscopy image is shown in Fig. 2D. The thickness of the MoS_2 flake was measured to be 25 nm.

The electron transport properties of the phototransistor are characterized at room temperature in air. Before the characterization, we took an I–V measurement on a blank nanopaper and estimated the leakage current to be <2 pA under 5 V (ESI†). Fig. 3A shows the I_{ds}–V_{ds} curves under four different gate biases, which are linear and symmetric, indicating good contact quality between the MoS_2 channel and Au electrodes. The lithography-free fabrication eliminates the need for adhesion metals and prevents contamination associated with wet processes, resulting in highly stable conductance and superior carrier mobility compared to the previous work (see the ESI†).[26,37]

The transfer curves (I_{ds}–V_{gs}) of the MoS_2 phototransistor are presented in Fig. 3B, revealing a typical n-type semiconducting behavior, which is consistent with previous reports.[4,6,8,9] Fig. 3C shows the I_{ds}–V_{ds} curves of the phototransistor when illumination is on (red) and off (black), respectively. Under stable and continuous illumination (532 nm, 15 μW), the incident laser can generate a significant photocurrent in the phototransistor. We compare the transfer characteristics with (red curve) and without (black curve) illumination as shown in Fig. 3D. In the dark state, the phototransistor shows a threshold voltage of V_t = 0.4 V, which shifts to V_t = 0.1 V when the illumination is on.

We further explored the photodetection performance of the device, characterized by its external photoresponsivity

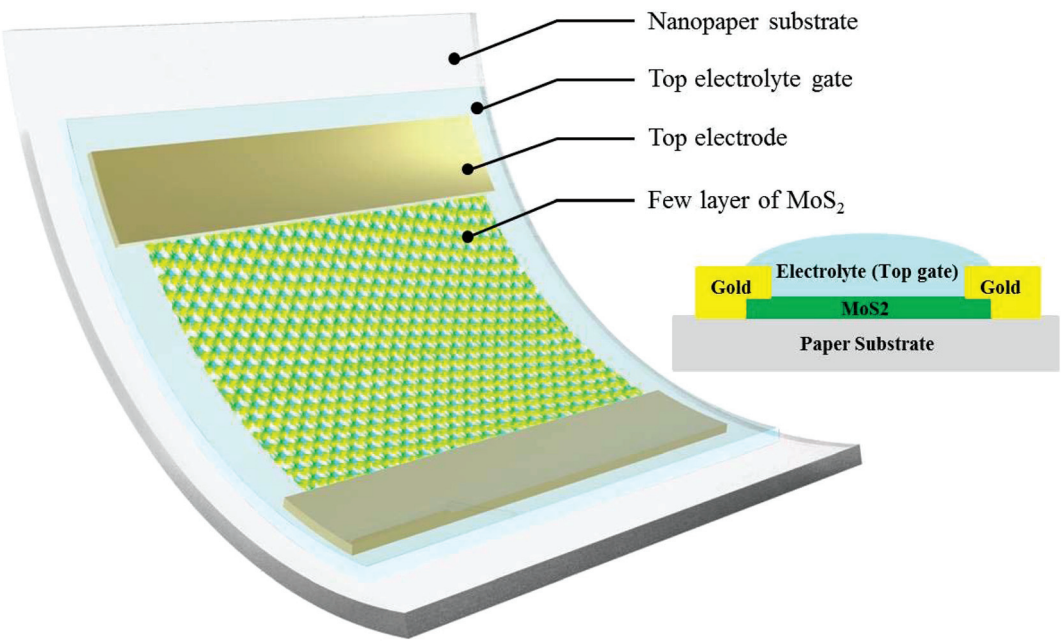

Fig. 1 Three-dimensional schematic and cross-sectional view of the MoS_2 phototransistor on transparent and flexible nanopaper (the top passivation layer is not included in this illustration).

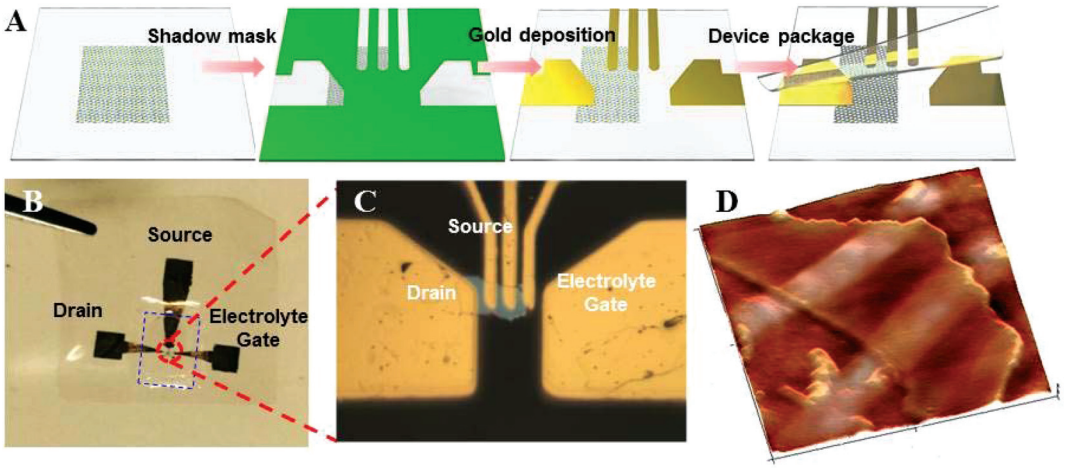

Fig. 2 A. Fabrication process of the phototransistor. B. Photograph of a sealed phototransistor. C. Optical image of zoom-in area of the phototransistor with MoS_2. D. An atomic force microscopy image of the phototransistor.

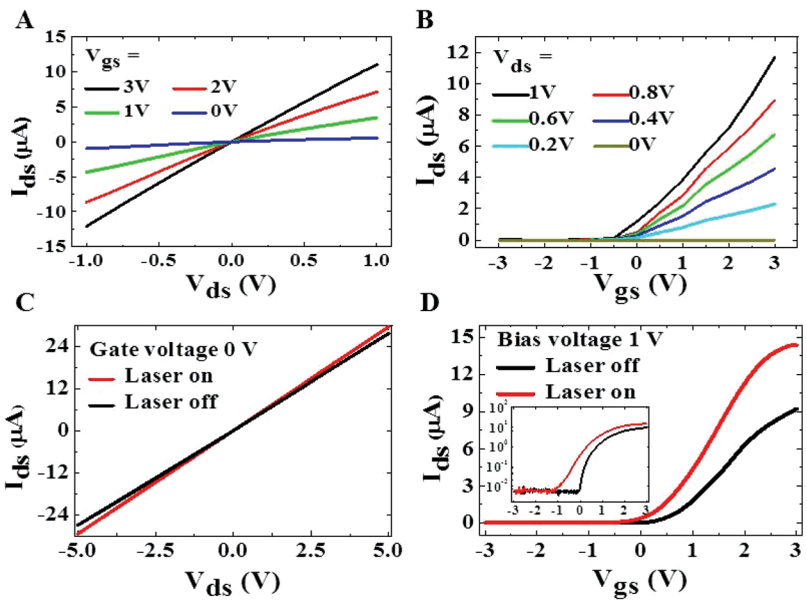

Fig. 3 Room temperature electrical and optoelectrical properties of the MoS_2 phototransistor. A. Output (I_{ds}–V_{ds}) characteristics of the phototransistor under different gate voltages. B. Room temperature transfer characteristics (I_{ds}–V_{gs}) of the same phototransistor at different source–drain biases. C. I_{ds}–V_{ds} at V_{gs} = 0 V before (black) and after (red) exposure to laser illumination. The power of the incident laser is 15 μW and the wavelength is 532 nm. D. Transfer characteristics (I_{ds}–V_{gs}) before (black) and after (red) exposure to laser. The inset shows the same data on a log scale.

R, defined as the ratio of the photocurrent (I_{pc}) and the incident illumination power (P_{in}):

$$R = \frac{I_{pc}}{P_{in}}$$

As shown in Fig. 4A, the responsivity decreases with the increasing illumination power (E), which is consistent with the observation in previous studies.[26] A quantitative correlation between R and E can be written[38] as:

$$R \sim E^{\beta-1}$$

The equation has been successfully applied to other phototransistors based on single-layer MoS_2, graphene and PbS.[37] By fitting the data (in the ESI†), we derived β to be 0.26. The parameter reflects the recombination dynamics of photoinduced carriers[39] and ranges between 0.2 to 0.7 in previous studies.[39,40] The decrease in responsivity with incident optical power is commonly observed in phototransistors according to other reports.[20,26,41] This effect is presumably associated with a reduction of the number of photogenerated carriers available for extraction under high photon flux due to Auger processes or the saturation of recombination and trap states that influ-

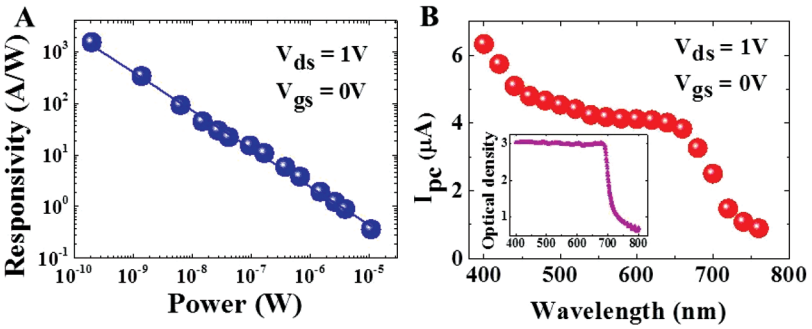

Fig. 4 Photoresponse of the MoS_2 phototransistor. A. Photoresponsivity of the device as a function of illumination power. The fitting uses $\sim E^{\beta-1}$, where E is the illumination power; β is the constant. B. Photocurrent of the same MoS_2 device at different wavelengths under V_{ds} = 1 V and V_{gs} = 0 V. The inset shows the absorption curve of MoS_2.

ence the lifetime of the generated carriers.[39] In addition, we note that the responsivity of our device is considerably higher than the average value reported in the literature. The maximum value reached 1.5 kA W^{-1} at 10 nW illumination power (see the ESI† for more information), while the highest responsivity measured with back gated MoS_2 phototransistors is typically below 1 kA W^{-1}.[26,30] We believe that both lithography-free fabrication and electrolyte gating contribute to the responsivity enhancement, and the latter plays a more dominant role. The electrolyte we used is a liquidized salt that contains cations (Li^+).[33] The cations accumulate on the MoS_2 surface under an externally applied voltage, forming an electric double layer (EDL). The EDL can effectively screen charge impurities and reduce electron scattering, thereby largely boosting the carrier mobility by 1 to 2 orders of magnitude.[42] At the same time, the electrolyte can also induce strong band bending at the MoS_2/Au interface and significantly lower the Schottky barrier.[43,44] The large enhancement in both intrinsic and extrinsic mobilities is presumably the reason for the exceedingly high responsivity observed in our phototransistors.

We have also measured the dark/light current across a wide range of wavelengths (Fig. 4B). When the incident laser is above 685 nm, the photocurrent drops sharply with the increasing wavelength. The transition around 685 nm corresponds to the excitation of electrons across the bandgap (1.81 eV) of multilayered MoS_2. The same transition is also evidenced in the absorption curve in the inset. Below 685 nm, the slow and monotonic increase in photocurrent with decreasing wavelength (or increasing photon energy) is presumably due to the fact that higher energy photons can excite electrons to higher energy states, resulting in a larger number of photocarriers that can overcome local energy barriers in the conduction channel and/or at the MoS_2/metal interface.

Besides excellent photoresponsivity, the phototransistor is highly transparent and flexible at the same time. In Fig. 5A, we compare the optical transmittance of the device (red curve) with a sheet of bare nanopaper (black curve) across a broad spectral range from 400 nm to 1100 nm. When compared at 550 nm, the optical transmittance of the phototransistor (82%) is slightly lower than that of the bare nanopaper (85%) due to

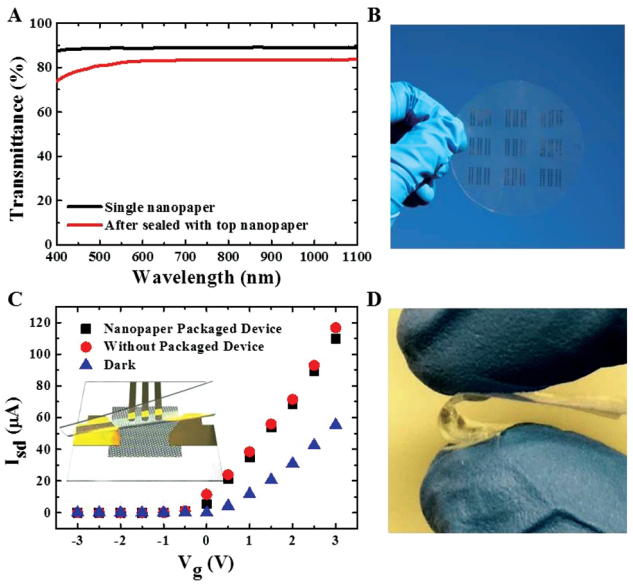

Fig. 5 Optical transmittance, transparency and flexibility of the MoS_2 phototransistor. A. Optical transmittance of a single sheet of nanopaper (black line) and a MoS_2 phototransistor sandwiched between two layers of nanopaper (red line). B. Photograph of an array of phototransistors showing high transparency. C. Transfer characteristics of the phototransistor without illumination (blue), under illumination but without passivation (red), and with both illumination and passivation (black). D. The device can be largely bended, exhibiting great flexibility.

the addition of a gel-electrolyte and a passivation layer. Fig. 5B and D demonstrate the excellent flexibility of the device and its compatibility with large-scale integration. The electrical and photodetection properties remain nearly the same before and after bending (in the ESI†). To verify that the passivation layer induces negligible perturbation to the phototransistor, we have recorded the transfer curves before and after passivation (Fig. 5C). In the dark state, the two devices behave the same as indicated by the data points in the blue triangle. Under illumination (532 nm), the bare device shows a slightly higher current compared to that at the same gate bias. The difference at V_{gs} = 3 V is approximately 6 μA between the two devices. The

result is in good agreement with the optical transmittance response as shown in Fig. 5A, in which the sealed phototransistor has a slightly lower optical transmittance and therefore is less sensitive to the incident laser.

Summary

We have demonstrated an electrolyte gated phototransistor based on multilayered MoS_2. The device uses highly transparent, flexible and biodegradable nanopaper as both the supporting substrate and passivation layer. It exhibits an excellent photoresponsivity of approximately 1.5 kA W^{-1} under 10 nW illumination power, considerably higher than typical back gated phototransistors reported in other studies. The device functions across a broad spectral range with excellent stability under sustained voltage bias and illumination. These properties make the device highly attractive for various industrial applications including touch sensor panels, image sensors, solar cells, and intelligent displays.

Experimental section

Fabrication of transparent nanopaper

The nanopaper was fabricated by previously established method published by Zhu *et al.*[8] The experimental procedure includes three major steps: (2,2,6,6-tetramethylpiperidin-1-yl) oxyl (TEMPO) oxidation reaction, Büchner filtration, and disintegration through a microfluidizer (M110 EH, Microfluidics Inc., USA). TEMPO-mediated oxidation was started by adding and dissolving 78 mg TEMPO into 25 mL buffer solution. The buffer consists of 0.08 M sodium carbonate (Na_2CO_3), and 0.02 M sodium bicarbonate ($NaHCO_3$). Three solutions, that is, 78 mg TEMPO in 25 mL buffer, 514 mg of sodium bromide (NaBr) in 50 mL buffer and 5 g dry weight of Kraft bleached softwood pulp in 115 mL buffer solution were combined. The solution was stirred at a speed of 700 rpm with an IKA RW20 digital mixer for 10 min followed by drop-wise addition of 35 mL sodium hypochlorite (NaClO). The pH value of the solution was measured every 20 min and kept at pH = 10.5 by adding 3 M sodium hydroxide (NaOH) for 2 hours. The reaction with continuous stirring at 700 rpm lasted overnight at room temperature. Then, the TEMPO-oxidized fibers were transferred to a vacuumed flask and funnel for Büchner filtration using a 0.65 μm nitrocellulose ester filter (Millipore DAWP29325) to wash away the reagents. Fiber was washed with 1 L deionized (DI) water by stirring at 800 rpm for 30 min and passing through a Büchner funnel into a flask twice. The resulting fiber cake was dissolved in DI water to form a 1 wt% solution and passed through a microfluidizer with thin z-shaped chambers. The channel dimension was 200 μm and the process pressure was 25 000 psi. After passing through the microfluidizer the fibers were dispersed in water to create a 1 wt% nanofibrillated cellulose (NFC) solution. The NFC solution was further diluted with DI water to 0.2 wt% and mixed at 500 rpm for 10 min with an IKA RW20 digital mixer. After that, the dispersion was degassed in a bath sonicator for 20 min, and passed through a 0.65 μm pore size nitrocellulose water filter (Millipore DAWP29325). The cake formed was compressed between a PET film (on top) and papers supported by an iron plate (below). Then, it was transferred to a hot pressing machine at 105 °C for 4–5 days to form nanopaper with a fiber diameter of about 5 nm.

References

1 Y. H. Jung, T.-H. Chang, H. Zhang, C. Yao, Q. Zheng, V. W. Yang, H. Mi, M. Kim, S. J. Cho, D.-W. Park, H. Jiang, J. Lee, Y. Qiu, W. Zhou, Z. Cai, S. Gong and Z. Ma, *Nat. Commun.*, 2015, **6**, 7170.
2 J. Huang, H. Zhu, Y. Chen, C. Preston, K. Rohrbach, J. Cumings and L. Hu, *ACS Nano*, 2013, **7**, 2106–2113.
3 A. Kulachenko, T. Denoyelle, S. Galland and S. B. Lindstrom, *Cellulose*, 2012, **19**, 793–807.
4 H. Zhu, Z. Xiao, D. Liu, Y. Li, N. J. Weadock, Z. Fang, J. Huang and L. Hu, *Energy Environ. Sci.*, 2013, **6**, 2105–2111.
5 W. A. MacDonald, M. K. Looney, D. MacKerron, R. Eveson, R. Adam, K. Hashimoto and K. Rakos, *J. Soc. Inf. Disp.*, 2007, **15**, 1075–1083.
6 D. O. Carlsson, G. Nystrom, Q. Zhou, L. A. Berglund, L. Nyholm and M. Stromme, *J. Mater. Chem.*, 2012, **22**, 19014–19024.
7 Z. Fang, H. Zhu, Y. Yuan, D. Ha, S. Zhu, C. Preston, Q. Chen, Y. Li, X. Han, S. Lee, G. Chen, T. Li, J. Munday, J. Huang and L. Hu, *Nano Lett.*, 2014, **14**, 765–773.
8 H. Zhu, S. Parvinian, C. Preston, O. Vaaland, Z. Ruan and L. Hu, *Nanoscale*, 2013, **5**, 3787–3792.
9 I. Siro, D. Plackett, M. Hedenqvist, M. Ankerfors and T. Lindstrom, *J. Appl. Polym. Sci.*, 2011, **119**, 2652–2660.
10 H. Zhu, Z. Fang, C. Preston, Y. Li and L. Hu, *Energy Environ. Sci.*, 2014, **7**, 269–287.
11 M. Nogi, C. Kim, T. Sugahara, T. Inui, T. Takahashi and K. Suganuma, *Appl. Phys. Lett.*, 2013, **102**, 181911.
12 M. Nogi, S. Iwamoto, A. N. Nakagaito and H. Yano, *Adv. Mater.*, 2009, **21**, 1595–1598.
13 T. Saito and A. Isogai, *Biomacromolecules*, 2004, **5**, 1983–1989.
14 T. Saito, Y. Okita, T. T. Nge, J. Sugiyama and A. Isogai, *Carbohydr. Polym.*, 2006, **65**, 435–440.
15 A. Isogai and Y. Kato, *Cellulose*, 1998, **5**, 153–164.
16 D. Klemm, F. Kramer, S. Moritz, T. Lindstrom, M. Ankerfors, D. Gray and A. Dorris, *Angew. Chem.,Int. Ed.*, 2011, **50**, 5438–5466.
17 R. T. Olsson, M. A. S. A. Samir, G. Salazar-Alvarez, L. Belova, V. Strom, L. A. Berglund, O. Ikkala, J. Nogues and U. W. Gedde, *Nat. Nanotechnol.*, 2010, **5**, 584–588.
18 H. Fukuzumi, T. Saito, T. Wata, Y. Kumamoto and A. Isogai, *Biomacromolecules*, 2009, **10**, 162–165.

19 J. P. Colinge, *Silicon-on-Insulator Technology: Materials to VLSI*, Springer, 3rd edn, ch. 1, 2004.
20 Z. Y. Yin, H. Li, H. Li, L. Jiang, Y. M. Shi, Y. H. Sun, G. Lu, Q. Zhang, X. D. Chen and H. Zhang, *ACS Nano*, 2012, **6**, 74–80.
21 W. G. Luo, Y. F. Cao, P. G. Hu, K. M. Cai, Q. Feng, F. G. Yan, T. F. Yan, X. H. Zhang and K. Y. Wang, *Adv. Opt. Mater.*, 2015, **3**, 1418–1423.
22 S. C. Dhanabalan, J. S. Ponraj, Q. Bao and H. Zhang, *Nanoscale*, 2016, **8**(12), 6410–6434.
23 H. Zhang, *ACS Nano*, 2015, **9**(10), 9451–9469.
24 H. Li, J. Wu, Z. Yin and H. Zhang, *Acc. Chem. Res.*, 2014, **47**(4), 1067–1075.
25 X. Huang, Z. Zeng and H. Zhang, *Chem. Soc. Rev.*, 2013, **42**(16), 1934–1946.
26 W. Zhang, J. K. Huang, C. H. Chen, Y. H. Chang, Y. J. Cheng and L. J. Li, *Adv. Mater.*, 2013, **25**(25), 3456–3461.
27 W. Choi, M. Y. Choi, A. Konar, J. H. Lee, G. B. Cha, C. H. Soon, S. Kim, J. Kim, D. Jena, J. Joo and S. Kim, *Adv. Mater.*, 2012, **24**(43), 5832–5836.
28 P. Joensen, R. F. Frindt and S. R. Morrison, *Mater. Res. Bull.*, 1986, **21**, 457–461.
29 D. B. Velusamy, R. H. Kim, S. Cha, J. Huh, R. Khazaeinezhad, S. H. Kassani, G. Song, S. M. Cho, S. H. Cho, I. Hwang, J. Lee, K. Oh, H. Choi and C. Park, *Nat. Commun.*, 2015, **6**, 8063.
30 F. H. L. Koppens, T. Mueller, Ph. Avouris, A. C. Ferrari, M. S. Vitiello and M. Polini, *Nat. Nanotechnol.*, 2014, **9**, 780–793.
31 S. Kim, A. Konar, W. S. Hwang, J. H. Lee, J. Lee, J. Yang, C. Jung, H. Kim, J. B. Yoo, J. Y. Choi, Y. W. Jin, S. Y. Lee, D. Jena, W. Choi and K. Kim, *Nat. Commun.*, 2012, **3**, 1011.
32 Q. H. Wang, K. K. Zadeh, A. Kis, J. N. Coleman and M. S. Strano, *Nat. Nanotechnol.*, 2012, **7**, 669–712.
33 X. Cai, A. B. Sushkov, M. M. Jadidi, L. O. Nyakiti, R. L. Myers-Ward, D. K. Gaskill, T. E. Murphy, M. S. Fuhrer and H. D. Drew, *Nano Lett.*, 2015, **15**, 4295–4302.
34 Y. J. Zhang, J. T. Ye, Y. Yomogida, T. Takenobu and Y. Iwasa, *Nano Lett.*, 2013, **13**, 3023.
35 E. Lhuillier, A. Robin, S. Ithurria, H. Aubin and B. Dubertret, *Nano Lett.*, 2014, **14**, 2715–2719.
36 G. Froehlicher and S. Berciaud, *Phys. Rev. B: Condens. Matter*, 2015, **91**, 205413.
37 J. Kwon, K. Y. Hong, G. Han, I. Omkaram, W. Choi, S. Kim and Y. Yoon, *Adv. Mater.*, 2015, **1**, 2224–2230.
38 Z. Sun, Z. Liu, J. Li, G. Tai, S.-P. Lau and F. Yan, *Adv. Mater.*, 2012, **24**, 5878–5883.
39 M. Buscema, D. J. Groenendijk, S. I. Blanter, G. A. Steele, H. S. Zant and A. Castellanos-Gomez, *Nano Lett.*, 2014, **14**, 3347–3352.
40 H. Xu, J. Wu, Q. Feng, N. Mao, C. Wang and J. Zhang, *Small*, 2014, **10**, 2300–2306.
41 H. S. Lee, S.-W. Min, Y.-G. Chang, M. K. Park, T. Nam, H. Kim, J. H. Kim, S. Ryu and S. Im, *Nano Lett.*, 2012, **12**, 3695–3700.
42 F. Wang, P. Stepanov, M. Gray, C. N. Lau, M. E. Itkis and R. C. Haddon, *Nano Lett.*, 2015, **15**, 5284–5288.
43 M. M. Perera, M.-W. Lin, H.-J. Chuang, B. P. Chamlagain, C. Wang, X. Tan, M. M.-C. Cheng, D. Tománek and Z. Zhou, *ACS Nano*, 2013, **7**(5), 4449–4458.
44 I. Popov, G. Seifert and D. Tomanek, *Phys. Rev. Lett.*, 2012, **108**, 156802.

